J MATER SCI 41 (2006) 913–925

Microstructure-based modeling of the deformation behavior of particle reinforced metal matrix composites

N. CHAWLA
Department of Chemical and Materials Engineering, Fulton School of Engineering, Arizona State University, Tempe, AZ 85287–6006
E-mail: nchawla@asu.edu

K. K. CHAWLA
Department of Materials Science and Engineering, University of Alabama at Birmingham, Birmingham, AL 35209
E-mail: kchawla@ual.edu

A review is provided of the use of analytical models and two dimensional (2D) and three dimensional (3D) microstructure based FEM models to accurately predict the properties of particle reinforced composite materials. It is shown that analytical models do not account for the microstructural factors that influence the mechanical behavior of the material. 2D models do capture the anisotropy in deformation behavior induced by anisotropy in particle orientation. The experimentally-observed dependence of Young's modulus and tensile strength is confirmed by the 2D microstructure-based numerical model. However, because of the 2D stress state, a realistic comparison to actual experimental values is not possible. A serial sectioning process can be used to reproduce and visualize the 3D microstructure of particle reinforced metal matrix composites. The 3D microstructure-based FEM accurately represents the alignment, aspect ratio, and distribution of the particles. Comparison with single particle and multiparticle models of simple shape (spherical and ellipsoidal) shows that the 3D microstructure-based approach is more accurate in simulating and understanding material behavior.

1. Introduction

The design and development of high performance materials requires a thorough understanding and careful control of microstructure and its effect on properties. This is particularly challenging given the multiphase and heterogeneous nature of most high performance composite materials. Modeling of the behavior of materials can be used as a versatile, efficient, and low cost tool for developing an understanding of material behavior. The robustness and accuracy of the model used can and should, of course, be verified by experimental results.

Particle reinforced metal matrix composites (MMCs) are an important class of composite materials [1–3]. These lightweight materials exhibit extremely high specific modulus, strength, and fatigue resistance, relative to conventional metals such as aluminum or titanium [3, 4]. In recent years, MMCs have replaced several established materials in military and commercial aircraft [1]. These materials are also aggressively being considered for applications in aeropropulsion, missiles, and electronic packaging in aircraft.

Conventional analytical [5, 6] and numerical techniques [7–9] have been developed and employed to understand the deformation behavior of particle reinforced composites. A review of current analytical and numerical techniques (presented in the next section), shows that while these methods have shed valuable insight into deformation behavior, they also simplify the heterogeneous microstructure of the composite. These simplifications make modeling and analysis more efficient and straightforward, for example, by minimizing computing resources. Nevertheless, it is well known that microstructural complexities such as the inhomogeneous spatial distribution of particles, irregular morphology of the particles, and anisotropy

0022-2461
DOI: 10.1007/s10853-006-6572-1

in particle orientation after secondary processing, such as extrusion, significantly affect deformation behavior. Thus, while conventional models can provide general knowledge of damage, they are unable to accurately predict the effective properties and local damage characteristics that are inherently dependent on microstructure. It follows that accurate prediction of macroscopic deformation behavior and an understanding of localized damage mechanisms can only really be accomplished by capturing the microstructure of the material as a basis for the model.

In this paper we review a novel methodology that addresses the critical link between microstructure and deformation behavior, by using two-dimensional (2D) [10–12] and three-dimensional (3D) [13–16] virtual microstructures as the basis for robust models that simulate damage caused by deformation. A review of analytical and conventional numerical modeling is first presented, followed by the main body of the paper, which addresses both 2D and 3D microstructure-based modeling. It is shown that 2D and 3D microstructure-based modeling approaches provide a quantitative understanding of localized damage phenomena, as well as excellent correlation to macroscopically-measured experimental behavior.

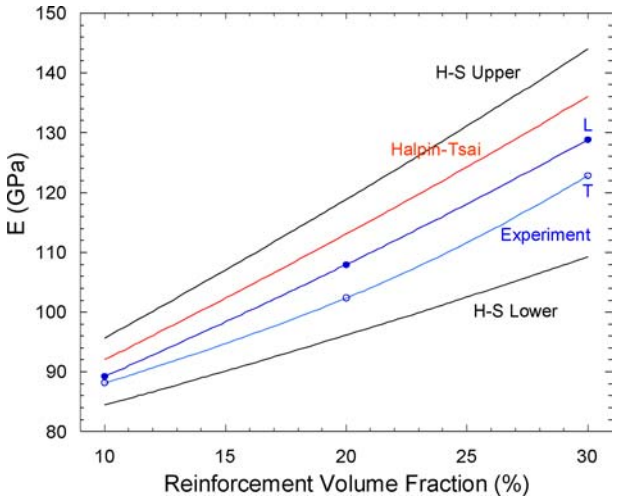

Figure 1 Effect of SiC particle fraction on the Young's modulus of SiC/Al composites. Analytical (Hashin-Shtrikman) and empirical (Halpin-Tsai) provide bounds, but are unable to predict the experimentally observed, microstructure-dependent anisotropy in modulus (L-longitudinal, T-transverse) [12].

2. Analytical and conventional numerical modeling

Modeling and prediction of the overall elastic-plastic response and local damage mechanisms in composite materials are very complex problems. Analytical and empirical models provide effective means of predicting the bounds on effective properties of the composite (e.g., Young's modulus) from the known properties of its constituents and for simple configurations of the phases [5, 6]. Fig. 1 shows the experimentally-determined Young's modulus of SiC particle reinforced Al matrix composites, as a function of SiC volume fraction. The composites show a distinct anisotropy in modulus along the extrusion axis (longitudinal, L) versus the transverse direction (T). Also shown are analytical bounds based on the models by Hashin-Shtrikman (H-S) and Halpin-Tsai (H-T). H-S treat the composite as an isotropic aggregate and the model is based on variational principles of linear elasticity, while H-T is a semi-empirical approach modified from continuous fibers to discontinuous reinforcement. This simple example shows that these models, while providing bounds on composite behavior, are not able to capture the anisotropy in composite behavior, because the microstructure of the composite is not really considered.

In particulate composite materials, numerical modeling is often more effective than analytical modeling since these materials lack the structural simplicity of continuous fiber composites or laminates and hence are not readily amenable to closed-form theoretical analyses. Another advantage of numerical modeling is that deformation and damage characteristics, particularly on a local scale, can be revealed. Numerical modeling of the behavior of composite materials has typically been conducted by assuming a single fiber, whisker, or particle of simple geometry in a unit cell model [7–9]. Modeling of damage in MMCs must take into consideration fracture of the ceramic reinforcement, void nucleation, growth and coalescence of voids within the metallic matrix, and/or decohesion and crack growth along the particle/matrix interface. Of these mechanisms, fracture of the reinforcement particles is quite important. Particular attention has been devoted to the fracture of reinforcing particles in the composite. Clearly, other failure mechanisms are also important, although a limited number of numerical studies have modeled matrix failure and interfacial effects [7]. Without invoking a damage model that can predict particle fracture *during* loading, the unit-cell models have been employed to directly study the effects of particle cracking on composite properties. These models represent an upper bound for particle damage (or lower bound for effective composite strength) wherein all the reinforcing particles in the composite are cracked. Similar calculations can be made for exploring the effects of particle fracture on the plastic response of the composite. Ghosh and co-workers [17, 18] modeled damage in the composite in 2D by approximating the particle morphology as ellipsoids, so the deformation assumed a two-dimensional stress or strain state (plane stress, plane strain, or modified plane strain). A 3D elastic Voronoi cell approach has also been reported, once again using ellipsoid particles [19].

Another important aspect of the microstructure in the composite is the effect of spatial distribution of the particles. The link between spatial distribution and mechan-

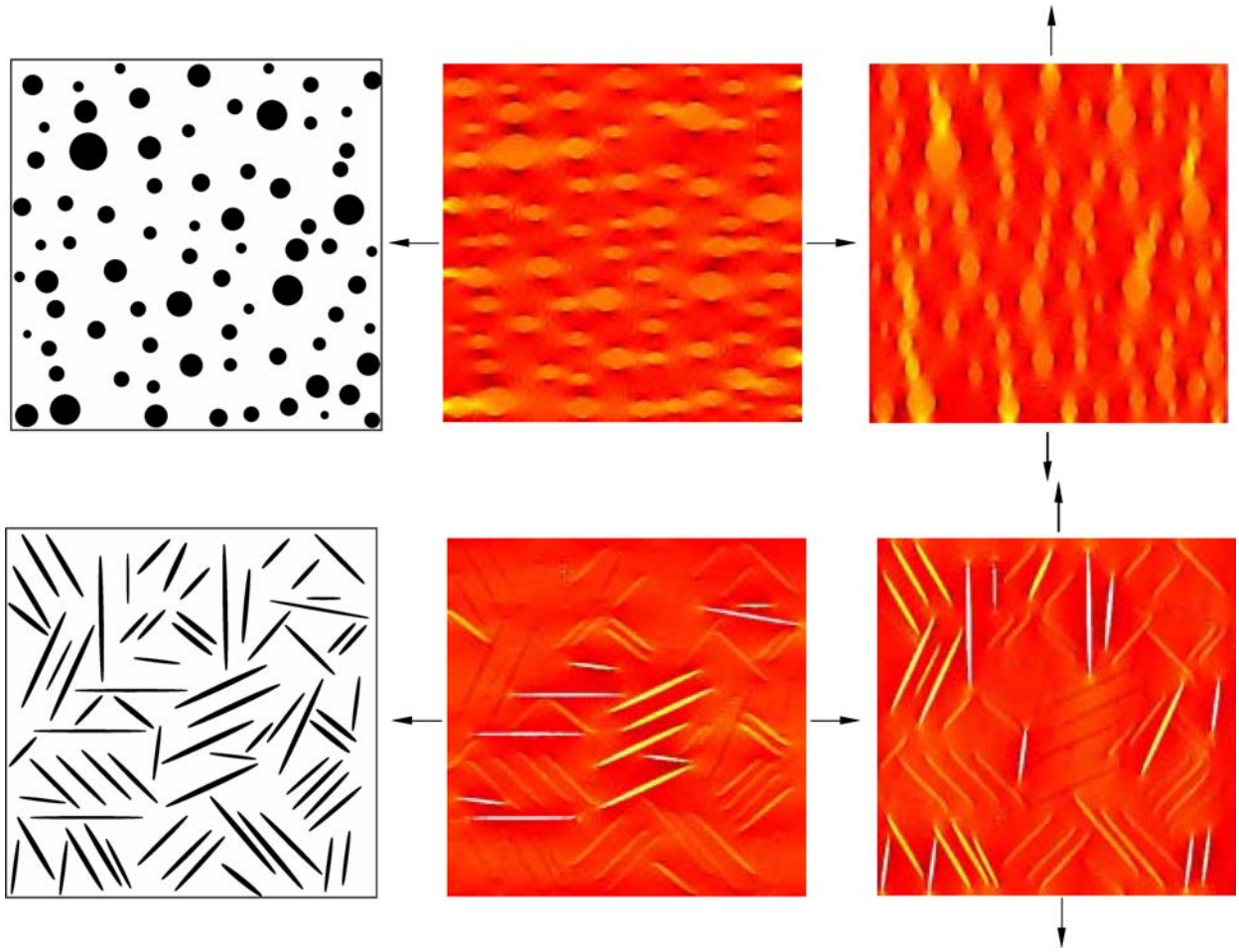

Figure 2 Effect of reinforcement shape on axial stress state (σ_{xx}) under uniaxial loading [22]: (a) homogeneous stress distribution for spherical particles and (b) inhomogeneous stress distribution for short fibers.

ical behavior has not been modeled extensively [20, 21]. Boselli *et al*. [20] modeled the effect of crack growth using idealized 2D microstructures, consisting of circular disks embedded in a metal matrix. It was found that clustering had a significant effect on the local shielding and "anti-shielding" effects at the crack tip. Segurado *et al*. [21] modeled the effect of particle clustering on damage in MMCs. The particles, modeled as spheres, were incorporated with different degrees of clustering (as quantified by a radial distribution function). It was shown that while the average stress in the particles did not vary significantly with clustering, the standard deviation in stress did. Thus, it was shown that for a given far-field applied stress in highly clustered composites, a given particle locally may have a much higher stress deviation from the average stress, and be more prone to fracture.

3. Microstructure-based modeling

3.1. Two-dimensional (2D) models

A simple illustration of the effect of composite microstructure on the local stress distribution during tensile loading is shown in Fig. 2 [22]. Fig. 2a shows a composite with perfect circular particles. The direction of loading does not change the stress distribution around the particles. Stress intensification is observed at the poles of the reinforcements. For a rigid spherical inclusion in a plastic matrix, the stress concentration occurs at the poles of the spherical reinforcement [23]. The local stress distribution for a composite with short fibers, however, is quite dependent on the direction of loading. Fibers that are favorably aligned with the loading axis exhibited a higher degree of load transfer, while those that are normal to the loading axis do not contribute much to composite strength. It should be noted, however, that the macroscopic deformation behavior of both types of composites is similar, because the reinforcement distribution is perfectly random. We now describe the principles and advantages of microstructure-based modeling using two examples of high performance particle reinforced metal matrix composites: (a) SiC particle reinforced Al alloy matrix composites and (b) WC particle reinforced Co matrix composites.

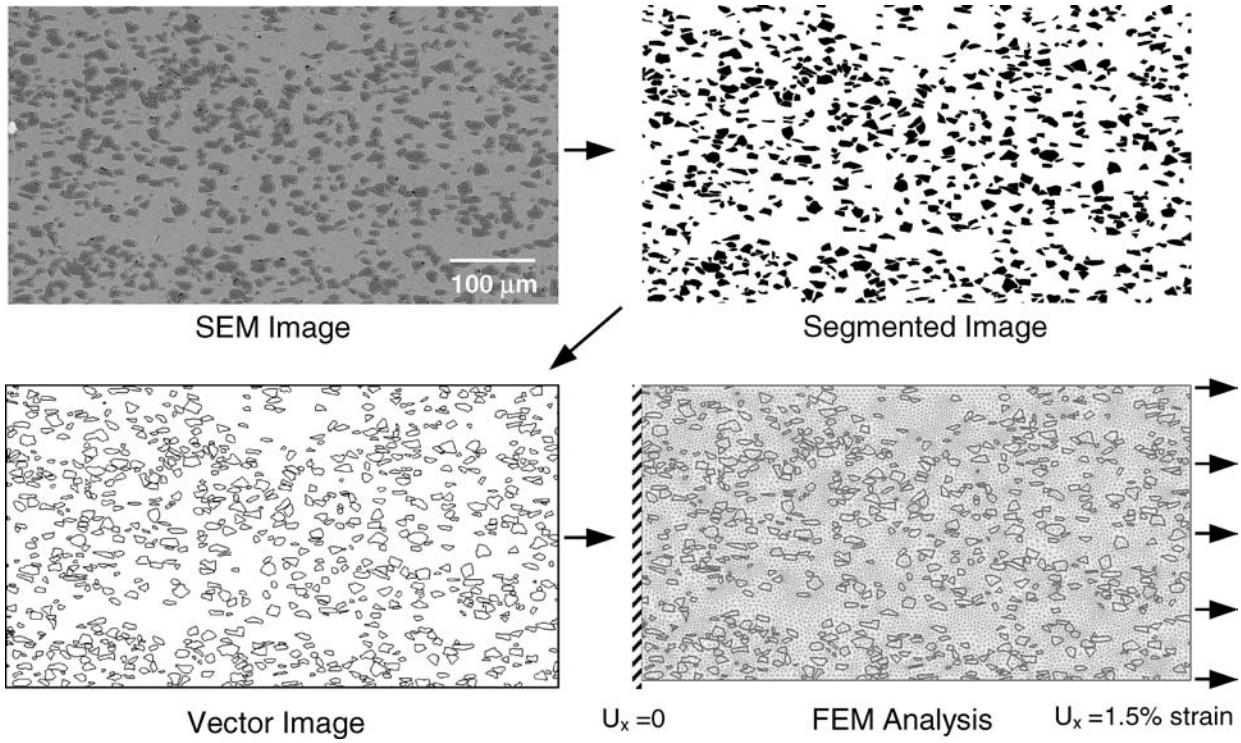

Figure 3 Schematic of process for using microstructure as a basis for numerical simulation ([12]). The digital image is segmented, converted to a vectorial format, and incorporated into FEM. u_x is the displacement in the x-direction.

3.2. SiC particle reinforced Al matrix composites

The model described above was carried out with a hypothetical microstructure. Actual microstructures, from optical or scanning electron microscopy (SEM) can be used as direct input to the FEM analysis. Ganesh and Chawla [12], for example, investigated the degree of orientation anisotropy of SiC particles, for a range of reinforcement volume fractions, in extruded SiC particle reinforced Al alloy composites. The influence of preferred orientation of reinforcement particles on tensile behavior was examined by two-dimensional SEM microstructures incorporated into FEM. The process for conducting the analysis is shown in Fig. 3. A representative microstructure[1] is segmented into a black and white image, which is further converted into vectorial format. The latter format can be input into the FEM software, so the model can now be meshed, the boundary conditions applied, and simulation conducted. In the work of Ganesh and Chawla [12], it was shown that the degree of particle orientation anisotropy was significant, and had a major effect on the anisotropy in tensile behavior, which was captured very well by the microstructure-based models.

Let us analyze the stress distribution in the SiC particle reinforced Al alloy matrix composite, under a uniaxial applied strain of 1%. Chawla *et al*. [10] conducted this particular analysis under linear elastic conditions. The classical shear-lag mechanism for load transfer in continuous fiber reinforced composites is clearly observed, despite the relatively low aspect ratio of the particles. Fig. 4a shows the stress within the particle and in the matrix immediately adjacent to the particle. Notice that a much higher stress is observed in the particle than in the matrix. Salient features of the microstructure on the stress distribution in the composite can also be obtained. Fig. 4b shows the intensification of stress in a clustered particle region. Note that the clustered region has a higher stress than the matrix region free of particles. Regions where particles touch are also sites of high stress concentration, and are thus more prone to crack initiation. The propensity of particle-to-particle contact also increases with volume fraction since the number of particles increases and the interparticle spacing decreases.

Plasticity of the matrix can also be incorporated, Fig. 5. The microstructure of an extruded 2080 Al matrix composite with 20 vol.% SiC particles is modeled. Note the preferential alignment of the particles along the extrusion axis. Here the constitutive law of the matrix was obtained from tensile experiments on the unreinforced Al alloy [24]. The stress distribution in the particles shows

[1]The definition of a representative microstructure is somewhat subjective. Clearly, the larger the microstructure modeled, the better the results. The computation efficiency of the model, however, decreases with increasing model size. One way to get around this is to model progressively larger microstructures, to determine that point at which the macroscopic and microscopic response remain unchanged.

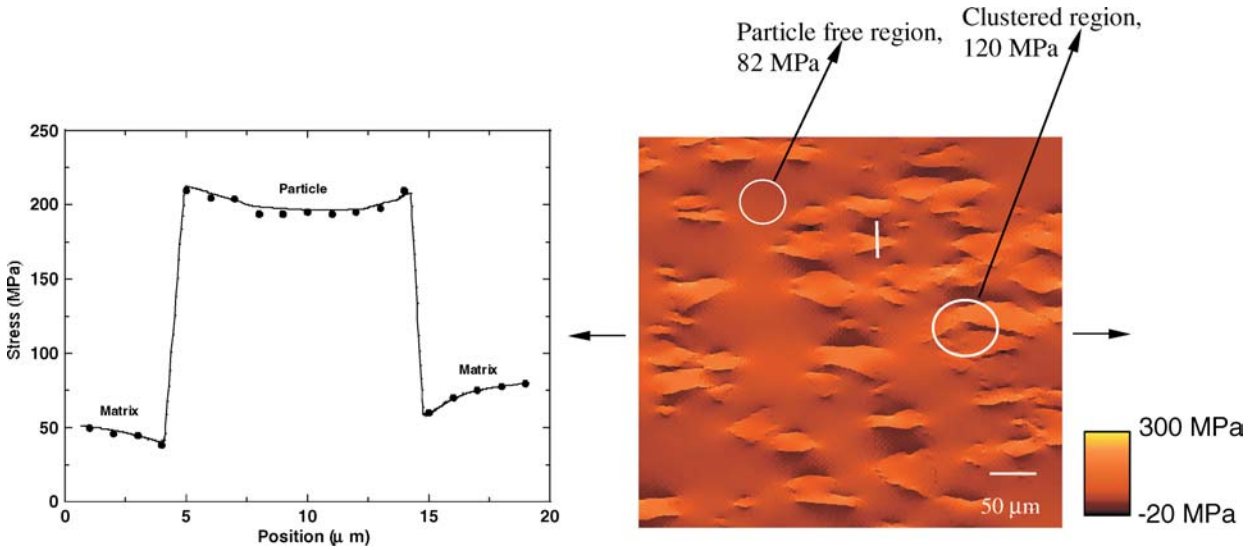

Figure 4 (a) Stress distribution (σ_{xx}) in a particle and particle/matrix interface of the composite; (b) stress map (Chawla *et al*. [10]). The white line in the stress map indicates the line scan over which the stress was computed. The particle is under a much higher stress than the matrix, indicating load transfer. The analysis is linear elastic.

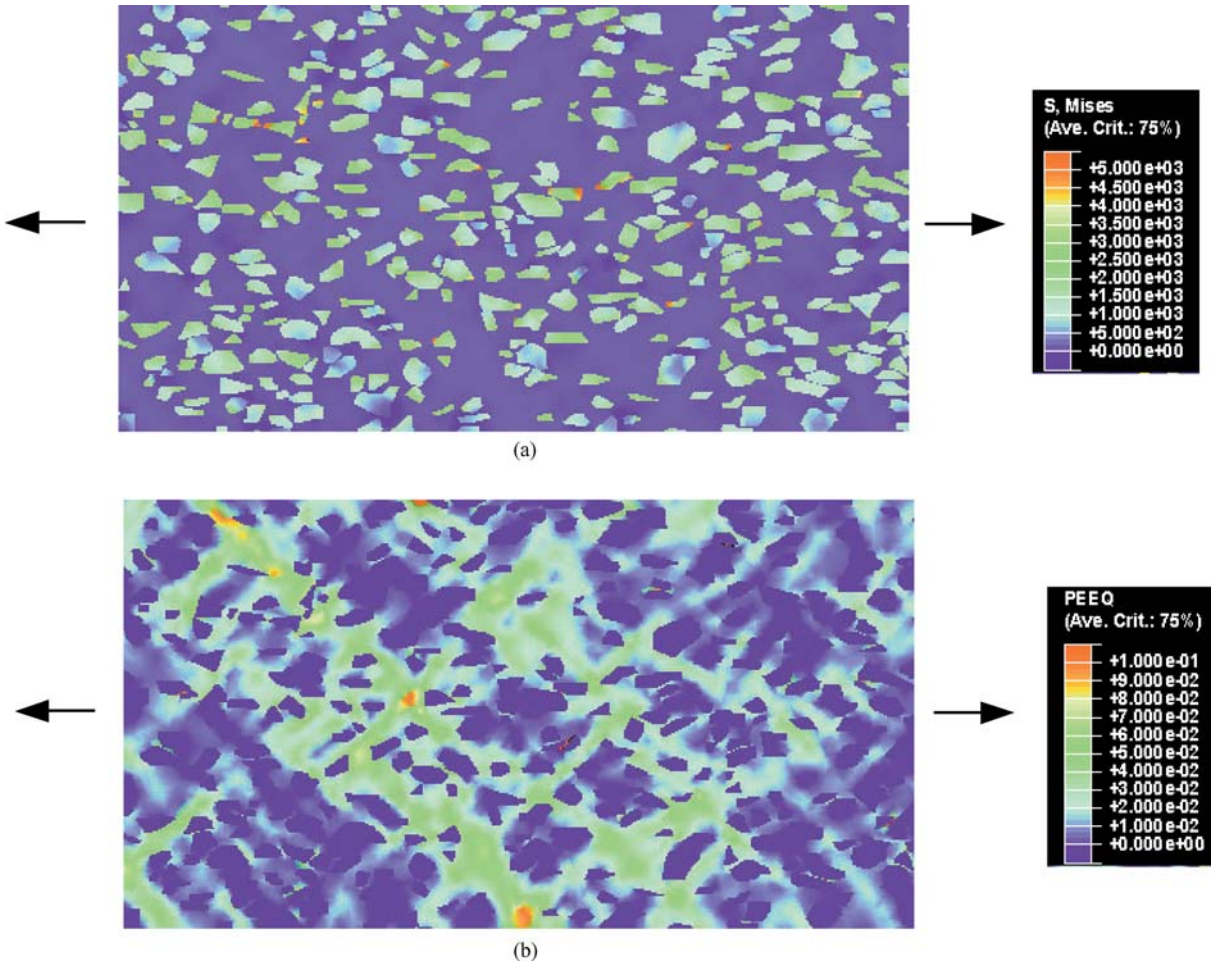

Figure 5 2D elastic-plastic microstructure-based model of a 2080 Al matrix composite with 20 vol.% SiC particles: (a) von Mises stress (MPa) and (b) equivalent plastic strain. The stress distribution in the particles shows that particles with higher aspect ratio, i.e., more rectangular particles, are under a higher stress. In addition, stress concentrations are present at the sharp corners of the particles. These high stress concentrations result in microplasticity in the matrix.

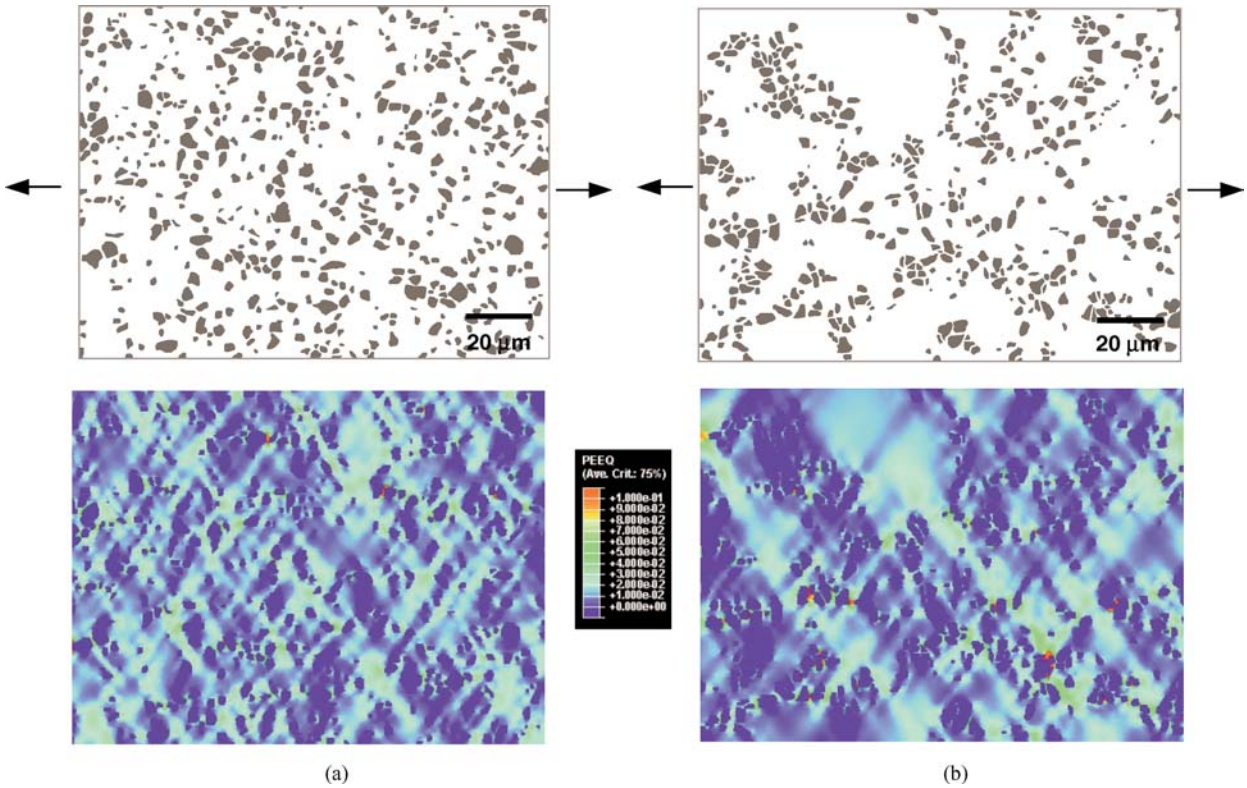

Figure 6 Effect of particle distribution on deformation behavior of SiC particle reinforced 2080 Al matrix composite: (a) homogeneous microstructure and (b) clustered microstructure. The distribution of plastic strain in the composite with homogeneous microstructure is much more uniform than in the clustered particle composite.

that particles with higher aspect ratio, i.e., more rectangular particles, are under a higher stress. In addition, stress concentrations are present at the sharp corners of the particles. As in the elastic case, stress concentrations are also observed at the poles of reinforcement, parallel to the loading direction. The plastic strain in the matrix is quite inhomogeneous. It appears to be most predominant in particle-free regions, where the matrix is allowed to shear. In particle clusters, where the interparticle spacing is decreased, the degree of triaxiality, due to constraint on the matrix, is increased. Therefore, in clustered particle regions the matrix is subjected to a higher stress, and very little matrix plasticity. The effect of clustering is more explicitly shown in Fig. 6. Here the degree of particle clustering in an Al/SiC/15_p was controlled by powder processing the composite with two Al-SiC particle size ratios: (a) Al/SiC ratio of 6.6 ($d_{Al} = 33\ \mu m$, $d_{SiC} = 5\ \mu m$) and (b) Al/SiC ratio of 1.4 ($d_{Al} = 7\ \mu m$, $d_{SiC} = 5\ \mu m$). Increasing Al/SiC ratio, of course, resulted in a greater degree of SiC clustering. In this example, one can clearly see that the distribution of plastic strain in the composite with homogeneous microstructure is much more uniform than in the clustered particle composite.

3.3. WC/Co double cemented carbides

Tungsten carbide/cobalt (WC/Co) composites, commonly known as cemented carbides, are one of the most important metal matrix composites used for their excellent wear resistance [25]. They are widely used for cutting, machining, and drilling purposes. Cemented carbides consist mainly of fine tungsten carbide particles and the binder metal cobalt. A novel particulate composite metal matrix composite called Double Cemented Carbide has been developed [26, 27]. This material consists of granules of WC/Co composite embedded within Co or another metal matrix as shown in Fig. 7. Thus, it is a kind of "dual" composite with a "composite-within-a-composite" structure. This concept provides microstructural design variables not available in conventional particulate metal matrix composites. These additional degrees of freedom enable remarkably enhanced *combinations* of properties, such as high toughness and wear resistance.

Figs. 7a and b show composites containing 75 vol.% WC particles in a cobalt matrix but with the two different types of structure: (a) conventional particulate composite structure with homogeneously distributed particles and (b) DCC structure. The DCC material has twice the toughness and six times the high-stress abrasive wear resistance than the conventional material, at the same total particle volume fraction. These improvements in properties result from the partitioning of the matrix to produce particle-free matrix regions separating the granular regions, which have higher particle volume fractions than the overall average. These ductile intergranular regions

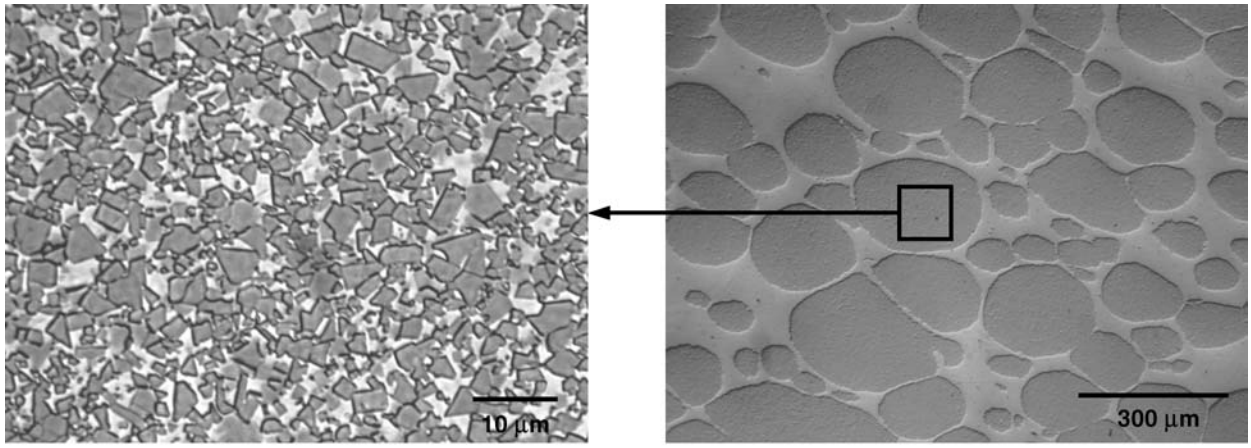

Figure 7 The double cemented (DC) carbide microstructure in (b) is envisioned to replace the conventionally cemented carbide microstructure in (a). Note the difference in magnification.

enhance fracture resistance with little detriment to abrasive wear resistance.

2D FEM simulations on microstructures acquired from these composites can be used to predict the modulus and thermal expansion behavior etc. [28]. In conventional cemented carbides, anomalous thermal expansion behavior is seen in composites with less than 20 vol.% matrix [29, 30]. This would appear to be attributable to the strong and stiff tungsten carbide network, which hinders the thermal expansion of highly constrained small amounts of Co. In this region of low cobalt content, it is likely that the high thermal expansion coefficient component, viz., cobalt does not significantly contribute to the overall thermal expansion. Thus, the thermal expansion behavior of the composite in this region is essentially that of pure polycrystalline WC. Since WC has a hexagonal structure, CTE of a polycrystalline WC is calculated via an orientational average of α for the a and c parameters.

Young's modulus and coefficient of thermal expansion measurements of the composites were determined in a manner similar to that described in the previous section. All SEM images were acquired in backscatter mode to provide for increased contrast between constituent phases. 2D elastic FEM analysis was conducted on several micrographs from one composite, until the results yielded a coefficient of variation below 0.05. In all composites, FEM analysis of six micrographs provided results, which exhibited a coefficient of variation below 0.05. As described in the previous section, the experimentally determined Young's modulus was compared with the elastic modulus bounds given by Hashin and Shtrikman [5]. The comparison between experimental, theoretical, and computational data is shown in Fig. 8. It appears that the 2D microstructure-based FEM and experimental results show a similar trend in Young's modulus as a function of vol.% matrix Co. The experimental and 2D FEM results both fall within the Hashin-Shtrikman bounds for composites with

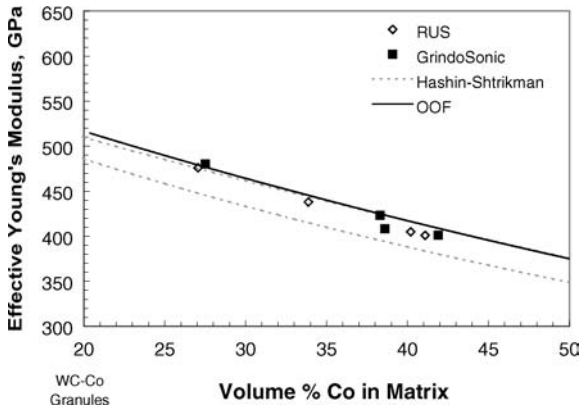

Figure 8 Experimental and computational results follow a similar decreasing trend in Young's modulus with increasing matrix Co content. Object oriented finite element (OOF) results provide a better estimation of dynamic Young's modulus than the HS prediction ([28]).

more than 38 vol.% Co. As the matrix content decreases, both FEM and experimental results start to deviate from the bounds. It is clear that in this range, the FEM better represents the trend in the experimental values of Young's modulus compared to the Hashin-Shtrikman bounds. This can be attributed to the microstructural features accounted for in the model, such as contiguity of the WC/Co granules.

A very important aspect of any particulate MMCs is the state of stress in as-fabricated state. Specifically, in the case of WC/Co composites, during cooling from 700°C to room temperature there develop large thermal stresses. Fig. 9 shows the stress distribution in conventional WC/Co and DCC. Note the high magnitude of compressive stress in WC, which is beneficial in the sense that in service in order to fracture the brittle WC in tension one must overcome the compressive stress. Note also that the magnitude of compressive stress is higher in the WC granules in DCC than in WC particle in conventional WC/Co.

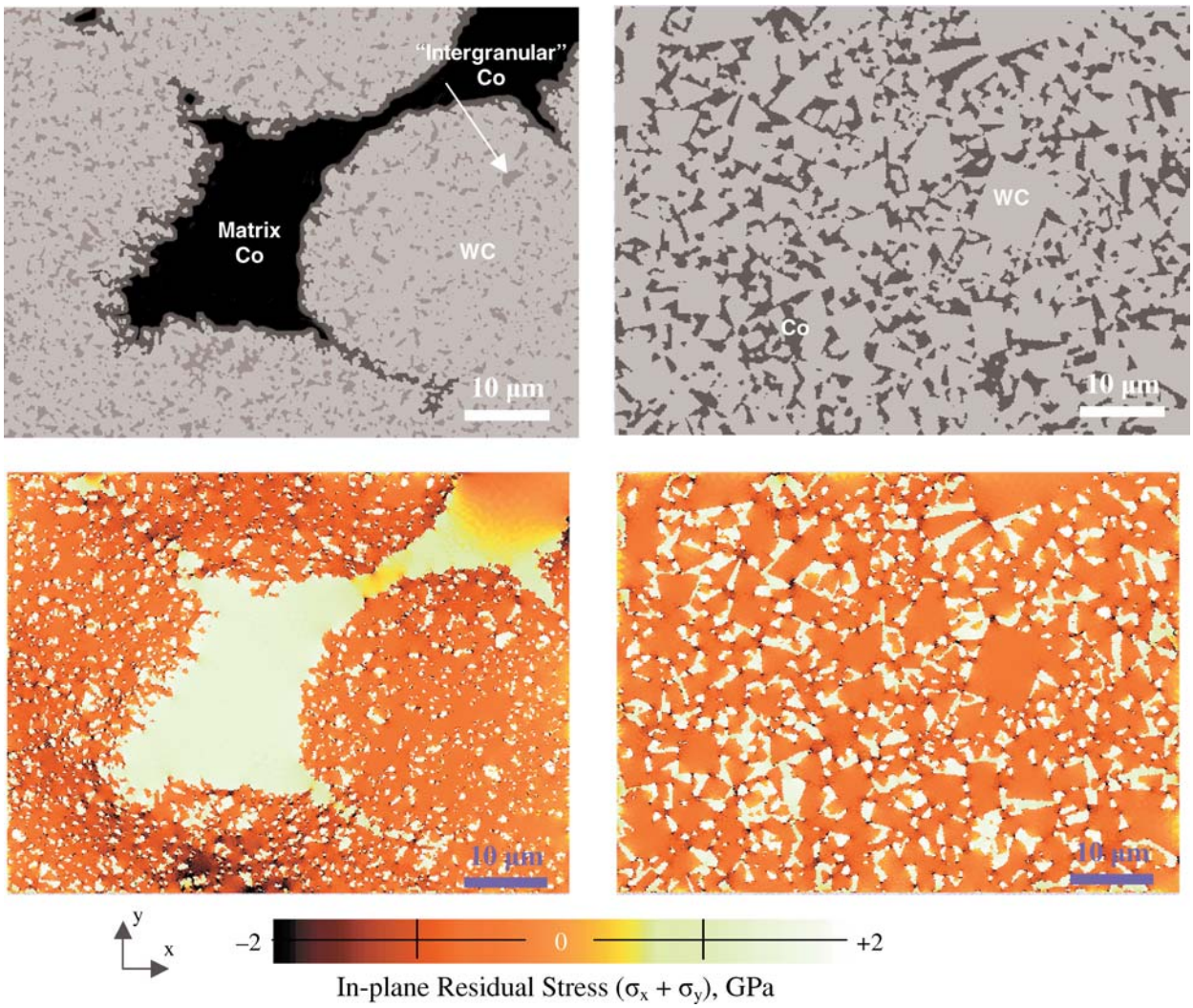

Figure 9 Stress distribution in conventional WC/Co (left hand column) and DCC (right hand column). Note the high magnitude of compressive stress in WC and that the magnitude of compressive stress is higher in the WC granules in DCC than in WC particle in conventional WC/Co.

4. Three-dimensional (3D) visualization and modeling

While 2D modeling can be used to obtain an understanding of deformation, the analysis must be carried out in either plane stress ($\sigma_z = 0$) or plane strain ($\varepsilon_z = 0$). This in itself is a simplification of the three-dimensional (3D) stress state in the actual material. In addition, using a 2D microstructure inherently implies that the particles are essentially modeled as disks. Thus, 3D analysis is necessary to obtain a true picture of the localized and macroscopic deformation. The 3D microstructure approach has two main components: Visualization and FEM modeling. In section 4.1 we discuss some approaches to obtain a 3D *virtual* microstructure, while section 4.2 describes 3D FEM modeling of deformation, using the virtual microstructure.

4.1. 3D visualization of microstructures

A few techniques have been used to obtain a 3D virtual microstructure, such as X-ray tomography [31, 32] and serial sectioning [33–42]. The serial sectioning concept involves the acquisition of several 2D sections through the thickness of the material, and 3D reconstruction of the microstructure using the 2D information. As a technique, serial sectioning has been used to visualize 3D object morphologies in a variety of fields, such as paleontology [33], biology [34, 35], and materials science [36–42]. Traditionally, serial sectioning used to consist of laborious, hand-drawn tracings of objects in the microstructure.

Recently, however, the evolution of computational capabilities has greatly simplified, enhanced the accuracy, and efficiency of the serial sectioning technique. Indeed, computer-aided serial sectioning techniques have allowed visualization and study of several material systems, including proeutectoid iron alloy [36], Al-Si [37], Sn-3.5Ag solder [38], and SiC/Al composites [13, 14, 39]. Alkemper and Voorhees [37] investigated the morphology of dendrites in 73 wt% Sn-Pb alloys, and quantified the radius of curvature of the dendritic morphology. The serial section-

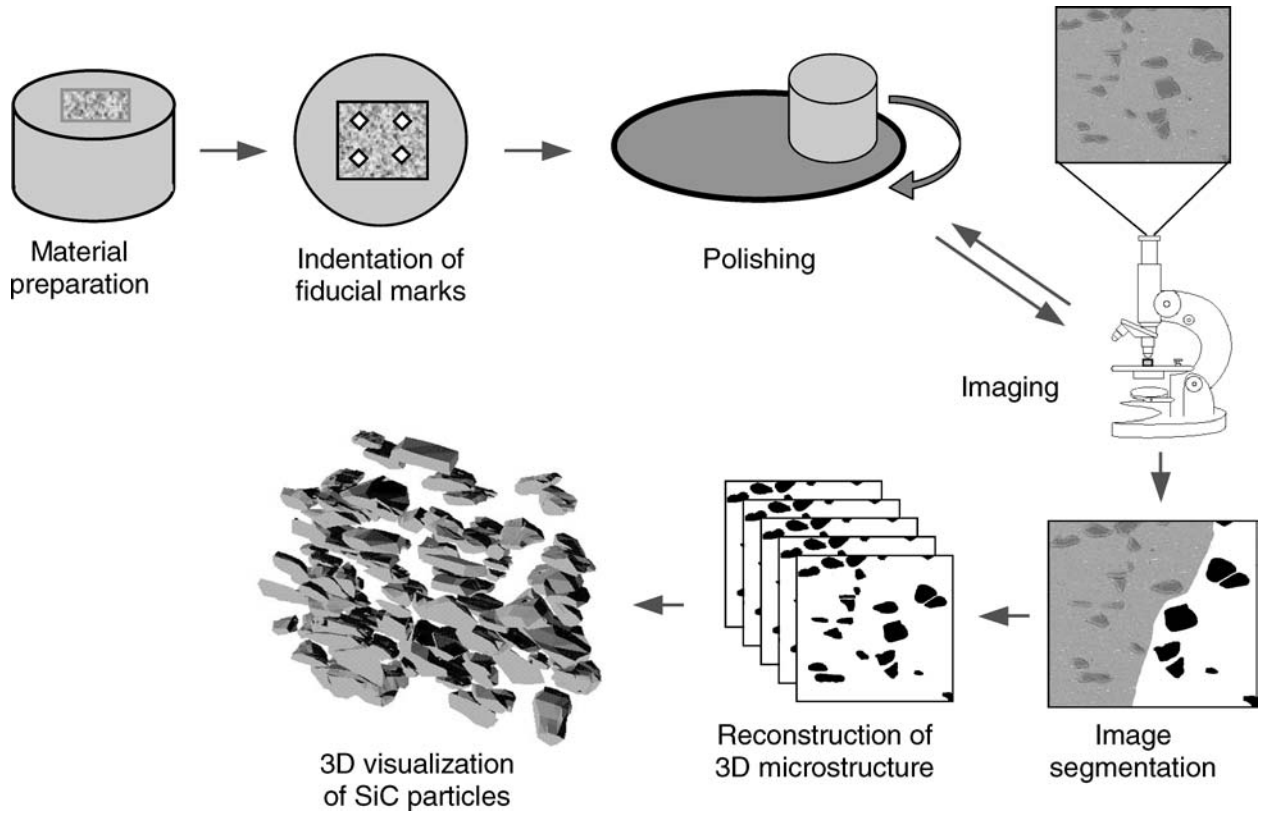

Figure 10 Flow chart of serial sectioning and 3D virtual microstructure generation process [14].

ing approach enabled improved results over 2D models by allowing visualization of the complex, interconnecting morphology of the microstructure. Kral and Spanos [40] and Lanzagorta *et al*. [41] used serial sectioning methods to examine the microstructure of Fe1.34C13.1Mn alloy using a combination of polishing/etching/SEM imaging. These authors used serial sectioning and reconstruction techniques to examine the morphology of cementite. Li *et al*. [17], Chawla *et al*. [13, 14], and Spowart *et al*. [39], have all used the serial sectioning technique to reconstruct the angular, irregularly shaped SiC particles in an Al matrix composite. Spowart *et al*. [39] have also developed a fully-automated robotic serial sectioning device that was custom-built for 3D characterization of advanced microstructures (Robo-Met.3D). The machine is capable of automatically performing metallographic serial sectioning at unprecedented rates and at slice thicknesses between 0.1 and 10 μm. Imaging is fully automatic, with the high-resolution digital images being combined using custom software to produce accurate 3-D datasets of the material microstructure in near real-time. In addition, chemical etching can be carried out automatically which increases the number of material systems that can be investigated, e.g. Ni-superalloys and high-strength titanium alloys.

In general, the following steps are used for the serial sectioning process and modeling, Fig. 10. The composite samples are cut and mounted. The first step is to choose a representative region of the microstructure. Selection of this region of interest is very important, but, as mentioned above, somewhat subjective. It is desirable to obtain a number of sections that encompass several SiC particles in a given volume, to allow entire particles to be reconstructed and incorporated in modeling. This volume is also dependent on the feature size (e.g., particle size). A volume of $100 \times 100 \times 20$ μm^3 yields approximately 100 particles, assuming that the SiC particles are approximately ~6–8 μm in diameter for a volume fraction of 20% SiC. This volume serves as a starting point for determining a "representative" number of particles for the FEM simulated response. Chawla *et al*. [16] have modeled the effect of microstructure size in modeling SiC particle reinforced Al alloy composite, and shown that above a minimum microstructure volume (in this case, corresponding to about 100 particles) the predicted response in unchanged.

4.2. Microstructure-based finite element modeling

In this section, we describe a methodology for incorporating the 3D virtual microstructure, obtained through serial sectioning, into a 3D elastic-plastic finite element model. We have used it successfully to model the behavior of SiC particle reinforced Al matrix composites [13, 14]. The refined 3D virtual model (after smoothing and re-

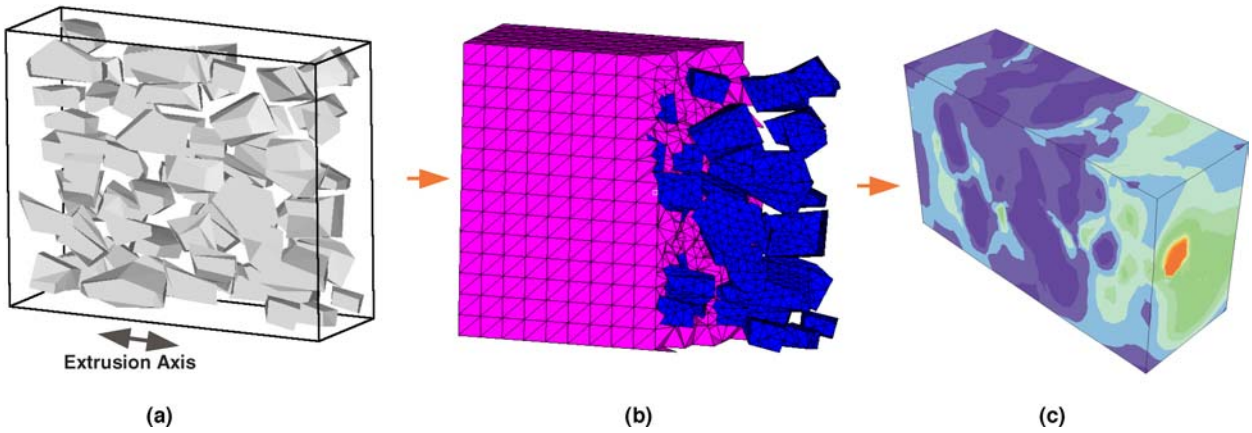

Figure 11 Methodology for 3D virtual microstructure-FEM analysis: (a) 3D microstructure reconstruction and visualization, (b) finite element mesh, and (c) finite element analysis of deformation.

fining the objects) is exported into pre-processor finite element meshing program (Hypermesh, Altair Engineering, Troy, MI) and then into a commercial finite element analysis program (ABAQUS/CAE Inc., Pawtucket, RI). Ten-noded, modified quadratic tetrahedral elements are typically used in the elastic-plastic analysis of the composite, particularly to conform to the irregular shape of the particles. Mesh refinement is conducted by gradually increasing the number of elements and quantifying the overall stress-strain curve, as well as local areas where the particles exhibit sharp corners. A typical number of elements in the 3D model is about 76,000 elements. All FEM analysis is conducted on a PC computer. Fig. 11 shows a typical volumetric mesh of a 50 particle model.

One of the challenges of using a microstructure-based approach is that a very large number of elements and a very refined mesh are required to conform to the heterogeneous nature of the microstructure. The larger the degree of simplification of the microstructure, of course, the more efficient the computation. A highly simplified microstructure model, however, will not capture the essential features of the microstructure. A comparison of the modeled 3D response using the actual microstructure versus a simplified representation of spherical and ellipsoids particles is shown in Fig. 12. The spatial distribution of the particles in both models is about the same. Note that the angular particles are under a much higher stress than the spherical and ellipsoidal particles, indicating more load transfer to the angular particles, Fig. 12b. The stress in the spherical particles is quite uniform, while that in the angular particles is not. The plastic strain contours in the matrix are also quite different, Fig. 12c. Less homogeneous plastic strain is observed in the model with angular particles, and the plastic strain distribution in the three models is very different. This simple comparison shows that the microstructure-based model predictions are, indeed, quite different from those of simplified spherical or ellipsoidal particles. Thus, modeling of the material using the actual microstructure is extremely important. It should be noted, that, in systems where the morphology of the second phase is relatively simple, such as spherical voids in cast Al [15], approximations to simple shapes can be made without sacrificing the accuracy of the model.

The advantage of using a 3D microstructure-based model is shown by a comparison of the overall stress-strain curve of the 3D microstructure simulation with experiment, and other unit cell and multiparticles simulations, Fig. 13. The microstructure-based model predicts the experimental behavior quite well. The other models are all clustered together, and predict lower strengthening than the experiment. More importantly, the localized plasticity that results from the sharp and angular nature of SiC particles, can only be captured in the microstructure-based model. It is interesting to note that multiparticle models consisting of spheres or ellipsoids do not constitute a substantial improvement over unit cell models.

The predicted Young's modulus of the composite, once again, shows that the microstructure-based model prediction is closest to the experiment [42], yielding a modulus of 108 GPa, Table I. The rectangular prism model prediction is also close to the experiment. This can be attributed to the larger decree of load transfer to a rectangular particle, relative to spherical or ellipsoidal particles. The lowest simulated moduli and strength were obtained by the unit cell sphere.

TABLE I Young's modulus predicted by various finite element models and comparison to experiment

Type of model	Young's modulus (GPa)
Experiment [42]	107.9 ± 0.7
3D Microstructure [14]	108
Unit cell – Rectangular prism [14]	107
Multiparticle – Spheres	106
Multiparticle – Ellipsods	106
Unit cell – Sphere [14]	100

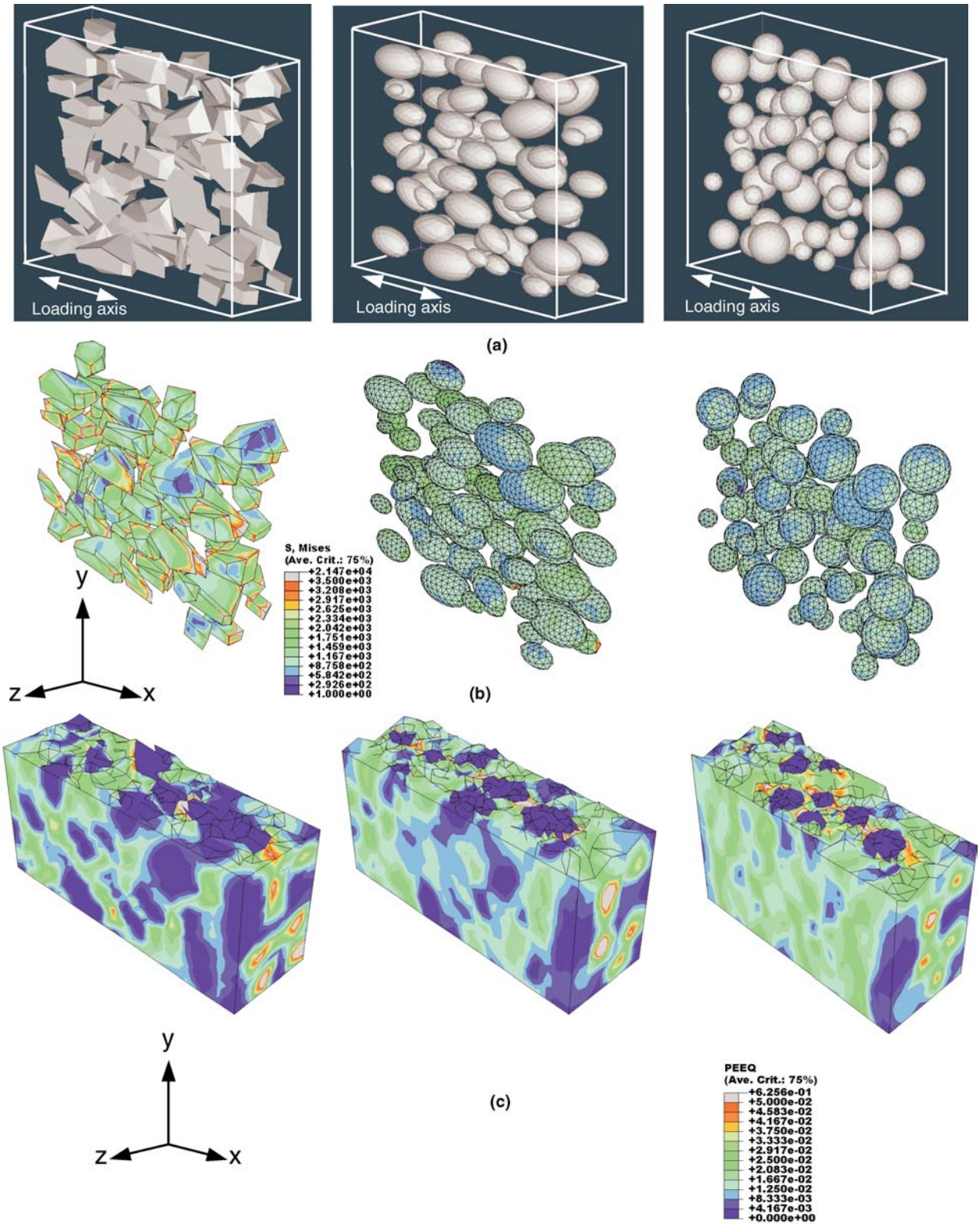

Figure 12 Comparison between 3D finite element models incorporation (i) actual microstructure and (ii) approximation to spherical particles: (a) FEM models, (b) von Mises stress distribution in particles, and (c) plastic strain in matrix. Note that the microstructure model exhibits much higher stress in the particles and larger and more inhomogeneous plastic strain than the simplified spherical particle model.

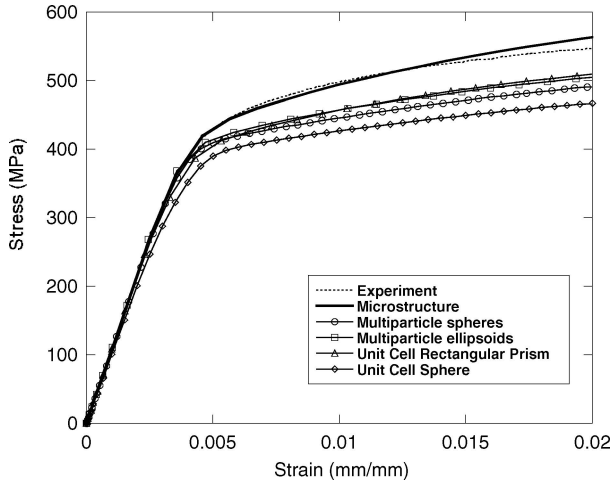

Figure 13 Comparison of stress-strain predictions from various FEM models after thermal cooling [14]. The 3D microstructure models (from two random regions in the microstructure) is most accurate in predicting the experimentally observed behavior.

5. Conclusions

The following conclusions can be made from this review of 2D and 3D microstructure-based finite element analysis of deformation in particle reinforced metal matrix composites:

- Analytical models are unable to accurately predict the properties of particle reinforced composite material since these models do not account for the microstructural factors that influence the mechanical behavior of the material.
- 2D microstructure based FEM modeling captures the anisotropy in deformation behavior and thermal resistance stresses. The experimentally-observed dependence of Young's modulus can be confirmed by the 2D microstructure-based numerical model. Because of the 2D stress state however, a realistic comparison to actual experimental values is not always possible.
- A serial sectioning process can be used to reproduce and visualize the 3D microstructure of particle reinforced metal matrix composites. The 3D microstructure accurately represents the alignment, aspect ratio, shape, and distribution of the particles.
- FEM simulation of the uniaxial loading behavior of particle reinforced metal matrix composites can be conducted using the 3D microstructure obtained from serial sectioning. When compared to 3D unit cell particles (spherical and rectangular prism) and multiparticle models of simple shape (spherical or ellipsoidal), the 3D microstructure models are most accurate in predicting the local and macroscopic uniaxial deformation behavior of the composite.
- The serial sectioning method, reconstruction, and 3D microstructure based FEM represent a significant improvement over 2D and 3D unit cell models, and can be effectively used to visualize and simulate of particle reinforced MMCs, as well as other complex heterogeneous materials behavior.

Acknowledgements

NC acknowledges partial financial support from the Office of Naval Research (Dr. A.K. Vasudevan, Program manager, Contract No. N000140110694). KKC acknowledges support from National Science Foundation (DMR 9904352).

References

1. N. CHAWLA and K. K. CHAWLA, "Metal Matrix Composites" (Springer, New York) (2006).
2. K. K. CHAWLA and N. CHAWLA, in "Kirk-Othmer Encyclopedia," (John-Wiley and Sons, New York, 2004).
3. N. CHAWLA and Y.-L. SHEN, *Adv. Eng. Mater.* **3** (2001) 357.
4. N. CHAWLA and J. E. ALLISON, in "Encyclopedia of Materials: Science and Technology," vol. 3, edited by B. Ilschner and P. Lukas (Elsevier Science, 2001) 2969.
5. Z. HASHIN and S. SHTRIKMAN, *J. Mech. Phys. Solids.* **11** (1963) 127.
6. J. C. HALPIN and S. W. TSAI, (1967) "Environmental Factors Estimation in Composite Materials Design," AFML TR 67.
7. J. LLORCA, A. NEEDLEMAN and S. SURESH, *Acta Metall. Mater.* **39** (1991) 2317.
8. J. R. BROCKENBROUGH, S. SURESH and H. A. WIENECKE, *Acta Metall. Mater.* **39** (1991) 735.
9. Y.-L SHEN, M. FINOT, A. NEEDLEMAN and S. SURESH, *Acta Metall. Mater.* **42** (1994) 77.
10. N. CHAWLA, B. V. PATEL, M. KOOPMAN, K. K. CHAWLA, R. SAHA, B. R. PATTERSON, E. R. FULLER and S. A. LANGER, *Mater. Charac.* **49** (2003) 395.
11. N. CHAWLA, B. JESTER and D. T. VONK, *Mater. Sci. Eng. A.* **A346** (2003) 266.
12. V. V. GANESH and N. CHAWLA, *Mater. Sci. Eng.* **A391** (2005) 342.
13. B. WUNSCH, X. DENG and N. CHAWLA, in "Computational Methods in Materials Characterisation," edited by A. A. Mammoli and C. A. Brebbia, (WIT Press, Boston, 2003) 175.
14. N. CHAWLA, V. V. GANESH and B. WUNSCH, *Scripta Mater.* **51** (2004) 161.
15. Z. SHAN and A. M. GOKHALE, *Acta Mater.* **49** (2001) 2001.
16. N. CHAWLA, R. S. SIDHU and V. V. GANESH, unpublished work.
17. M. LI, S. GHOSH, T. N. ROUNS, H. WEILAND, O. RICHMOND and W. HUNT, *Mater. Charac.* **41** (1998) 81.
18. M. LI, S. GHOSH and O. RICHMOND, *Acta Mater.* **47** (1999) 3515.
19. S. GHOSH and S. MOORTY, *Computa. Mech.* **34** (2004) 510.
20. J. BOSELLI, P. D. PITCHER, P. J. GREGSON and I. SINCLAIR, *Mater. Sci. Eng.* **A300** (2001) 113.
21. J. SEGURADO, C. GONZALEZ and J. LLORCA, *Acta Mater.* **51** (2003) 2355.
22. N. CHAWLA, F. OCHOA, V. V. GANESH, X. DENG, M. KOOPMAN, K. K. CHAWLA and S. SCARRITT, *J. Mater. Sci.- Mater. Elect.* **15** (2004) 385.
23. J. N. GOODIER, *J. Appl. Mech.* **55-7** (1933) 39.
24. N. CHAWLA, C. ANDRES, J. W. JONES and J. E. ALLISON, *Metall. Mater. Trans.* **29A** (1998) 2843.

25. G. S. UPADHYAYA, "Cemented Tungsten Carbides" (Noyes Publ, Westwood, NJ, 1998).
26. Z. FANG, G. LOCKWOOD and A. GRIFFO, *Metall. Mater. Trans.* **30A** (1999) 3231.
27. X. DENG, B. R. PATTERSON, K. K. CHAWLA, M. C. KOOPMAN, Z. FANG, G. LOCKWOOD and A. GRIFFO, *J. Refract. Met. Hard Mater.* **19** (2001) 547.
28. M. KOOPMAN, K. K. CHAWLA, C. COFFIN, B. R. PATTERSON, X. DENG, B. V. PATEL, Z. G. FANG and G. LOCKWOOD, *Adv. Eng. Mater.* **4** (2002) 37.
29. V. I. TUMANOV, V. F. FUNKE, M. L. BASKIN and J. A. NOVIKOVA, *Akademiya Nauk SSSR, Izvestiya, Metallurgiya, Gornoe Delo.* **1** (1964) 170.
30. J. GURLAND and J. T. NORTON, *Trans. AIME.* **194** (1952) 1052.
31. L. BABOUT, E. MAIRE, R. FOUGERES, *Acta Mater.* **52** (2004) 2475.
32. A. BORBÉLY, F. F. CSIKOR, S. ZABLER, P. CLOETENS and H. BIERMANN, *Mater. Sci. Eng.* **A367**. (2004) 40.
33. M. J. HERBERT and C. B. JONES, *Comp. Geosci.* **27** (2001) 427.
34. M. YANUKA, F. A. DULLIEN and D. E. ELRICK, *J. Micros.* **135** (1984) 159.
35. V. A. MOSS, D. MCEWAN JENKINSON and H. Y. ELDER, *J. Micros.* **158** (1990) 187.
36. M. V. KRAL and G. SPANOS, *Scripta Mater.* **36** (1997) 875.
37. J. ALKEMPER and P. W. VOORHEES, *J. Micros.* **201** (2001) 388.
38. R. S. SIDHU and N. CHAWLA, *Mater. Charac.* **52** (2004) 225.
39. J. E. SPOWART, H. M. MULLENS and B. T. PUCHALA, *JOM.* **10** (2003) 35.
40. M. V. KRAL and G. SPANOS, *Acta Mater.*, **47** (1999) 711.
41. M. LANZAGORTA, M. V. KRAL, J. E. SWAN II, G. SPANOS, R. ROSENBERG, E. KUO, IEEE Visualization '98 Conference Proceedings (1998) p. 487.
42. N. CHAWLA, C. ANDRES, J. W. JONES and J. E. ALLISON, *Metall. Mater. Trans.* **29A** (1998) 2843.